# Impacts of Central Pacific El Niño on Southern China Spring Precipitation Controlled by its Longitudinal Position

FENG JIANG, WENJUN ZHANG, AND XIN GENG

*Collaborative Innovation Center on Forecast and Evaluation of Meteorological Disasters, Key Laboratory of Meteorological Disaster of Ministry of Education, Nanjing University of Information Science and Technology, Nanjing, China*

MALTE F. STUECKER

*Center for Climate Physics, Institute for Basic Science, and Pusan National University, Busan, South Korea*

CHAO LIU

*Collaborative Innovation Center on Forecast and Evaluation of Meteorological Disasters, Key Laboratory of Meteorological Disaster of Ministry of Education, Nanjing University of Information Science and Technology, Nanjing, China*

(Manuscript received 4 April 2019, in final form 16 July 2019)

ABSTRACT

Here we investigate the response of boreal spring precipitation over southern China (SPSC) to central Pacific (CP) El Niño based on observational datasets. While there is enhanced precipitation over southern China during the decaying boreal spring of eastern Pacific (EP) El Niño events, so far no clear precipitation response has been detected during the same decaying stage for CP El Niño composites. Here we show that around half of the CP El Niño events coincide with enhanced SPSC (wet CP El Niño), while the other half are accompanied by reduced SPSC (dry CP El Niño). These two types of CP El Niño events bear dramatically different evolution features in their respective tropical sea surface temperature anomaly (SSTA) patterns. Wet CP El Niño events are characterized by an SSTA longitudinal position confined to the tropical central-eastern Pacific. In contrast, dry CP El Niño events exhibit a clear westward propagation of SSTAs during their evolution, with maximum SSTAs located to the west of the date line after their mature phase. These different longitudinal positions of positive SSTAs during their decaying phase result in distinct meridional structures of the tropical Pacific convection anomalies as well as the ENSO combination mode (C-mode) response. An anomalous low-level anticyclone is evident over the western North Pacific during wet CP El Niño events during their decaying phase, while an anomalous cyclonic circulation is found for dry CP El Niño events. We emphasize that the impacts of CP El Niño on the SPSC depend crucially on the simultaneous zonal location of warm SSTAs in the tropical Pacific.

## 1. Introduction

As an important transition period of the atmospheric circulation from winter to summer season, boreal spring usually corresponds to the first rainy season over southern China, known as the ''spring persistent rains'' (Tian and Yasunari 1998), accounting for more than 30% of the annual accumulation in this region (LinHo et al. 2008; Wu and Mao 2016). The spring precipitation over southern China (SPSC) exhibits large year-to-year variability, often associated with either severe droughts or floods, which often brings about substantial economic and agricultural losses (Murakami 1951; Lau and Li 1984; Chang et al. 2000a,b; Ding and Chan 2005). Studies on the SPSC variability and associated mechanisms carry important implications for regional seasonal prediction as well as disaster prevention and mitigation efforts.

It has been known that the SPSC variability is closely related to tropical sea surface temperature (SST) (e.g., Zhang et al. 1996; Wang et al. 2000; Wu et al. 2003; Terray et al. 2007; Feng et al. 2014). Furthermore, SPSC responses to snow cover variability over Eurasia and the Himalayas (e.g., Wu et al. 1996; Fasullo 2004; Wu and Kirtman 2007; Xin et al. 2010; Senan et al. 2016) and the

*Corresponding author*: Dr. Wenjun Zhang, zhangwj@nuist.edu.cn

DOI: 10.1175/JCLI-D-19-0266.1

Southern Hemisphere annular mode (Zheng et al. 2015) have been hypothesized. In particular, El Niño–Southern Oscillation (ENSO) exerts great impacts on the interannual SPSC variability (e.g., Huang and Wu 1989; Wang et al. 2000; Zhou and Wu 2010). As the predominant mode of climate variability arising from coupled air–sea interaction in the tropical Pacific (e.g., Cane and Zebiak 1985; Jin 1997; Neelin et al. 1998; Wallace et al. 1998; McPhaden et al. 2006; Timmermann et al. 2018), ENSO impacts East Asian climate through atmospheric teleconnections (e.g., Ropelewski and Halpert 1987; Fu and Teng 1988; Tao and Zhang 1998; Wallace et al. 1998; Wilson 2009; Wang et al. 2013; Zhang et al. 2014; Ng et al. 2019).

From El Niño developing fall to the following decaying summer, an anomalous lower-tropospheric anticyclone is evident near the Philippine Sea, which usually transports more moisture to southern China and thereby increases local precipitation (e.g., Zhang et al. 1996; Wang et al. 2000; Wang and Zhang 2002). Several dynamical mechanisms have been proposed to explain how ENSO affects the atmospheric circulation anomalies near the Philippine Sea. Early studies hypothesized that local SST cooling over the western tropical Pacific initiates the anomalous anticyclone over the western North Pacific (WNP) as a Rossby wave response (Wang et al. 2000). Recent studies demonstrated that an ENSO combination mode, arising from the interaction between ENSO and the warm pool annual cycle (Stuecker et al. 2013, 2015), is responsible for the development of WNP anticyclone and thus the enhancement of SPSC during the decaying year of traditional El Niño events (Zhang et al. 2015, 2016). In boreal summer, the transition to La Niña (Stuecker et al. 2015), local WNP air–sea coupling (Wang et al. 2000), and El Niño–induced delayed Indian Ocean warming (e.g., Watanabe and Jin 2002; Yang et al. 2007; Xie et al. 2009) play important roles in extending the lifetime of this anomalous circulation (Stuecker et al. 2015).

In recent decades, a new type of El Niño (the central Pacific type, hereafter CP El Niño) has been frequently detected in the central tropical Pacific, differing dramatically from the conventional El Niño (the eastern Pacific type, hereafter EP El Niño), which has an SST anomaly (SSTA) center in the eastern Pacific (e.g., Larkin and Harrison 2005; Ashok et al. 2007; Kao and Yu 2009; Weng et al. 2009; Yu and Kim 2010). A number of studies have demonstrated that the East Asian climate responses to CP El Niño events are considerably distinct from those to EP El Niño events (e.g., Feng et al. 2011; Wang and Wang 2013; Zhang et al. 2011, 2013, 2014; Xu et al. 2013, 2019). Specifically, during the El Niño decaying spring season, the SPSC is reduced in CP years, opposite to the precipitation increase that is usually observed during EP years (Feng and Li 2011). However, another study argued that no statistically significant ENSO signal can be detected during the CP El Niño decaying spring (Feng et al. 2011). One recent study documented that the composite atmospheric combination mode (C-mode) response to CP El Niño SSTA forcing does not exhibit a pronounced meridional asymmetry (Zhang et al. 2015), thus potentially explaining the absences of a WNP anomalous anticyclone and SPSC signal during CP El Niño events. Given these differing results, it seems that whether CP El Niño events can exert significant impacts on the SPSC is not well understood. In this study, we investigate the SPSC responses during CP El Niño events based on the latest observational datasets and find that around half the CP El Niño events correspond to enhanced SPSC (wet CP El Niño), while the other half are associated with reduced SPSC (dry CP El Niño). These different climate responses are closely associated with different longitudinal locations of positive SSTAs during the decaying spring seasons for the wet and dry CP El Niño events.

In the remainder of the paper, section 2 introduces the data and methodology. Section 3 displays the characteristics of SPSC during different flavors of decaying El Niño spring seasons. In section 4, the SSTA evolution of the two types of CP El Niño events are investigated and compared. Then, in section 5 we propose a possible mechanism that explains how different SSTA patterns associated with wet and dry CP El Niño events lead to distinct SPSC. Finally, a summary and discussion are provided in section 6.

## 2. Data and methodology

### a. Observations

In this study, the global sea ice and SST analyses (1971–2017) from the Hadley Centre (HadISST1) provided by the Met Office Hadley Centre are used (Rayner et al. 2003). The precipitation data from the Global Precipitation Climatology Centre (GPCC; 1971–2017) are utilized to investigate precipitation over land (Rudolf et al. 1994; Becker et al. 2013). We also use monthly 160 station gauge-based precipitation data (1971–2017) supplied by the China Meteorological Administration (CMA) to test the robustness of the GPCC data over southern China. In addition, the global precipitation (over land and ocean) product from the Climate Prediction Center Merged Analysis of Precipitation (CMAP) is used (Xie and Arkin 1996) to examine the convection anomalies over the tropical Pacific. CMAP precipitation is used only for the period of 1979–2017 because no data are available before 1979. To examine the variation of El Niño–related wind

TABLE 1. El Niño events for the 1971–2017 period.

| EP El Niño events | CP El Niño events |
|---|---|
| 1972/73, 1982/83, 1997/98, 2015/16 | 1977/78, 1979/80, 1986/87, 1991/92, 1994/95, 2002/03, 2004/05, 2006/07, 2009/10 |

anomalies, we use monthly 10-m winds (1971–2017) from the National Centers for Environmental Prediction (NCEP)–National Center for Atmospheric Research (NCAR) reanalysis dataset (Kalnay et al. 1996). The horizontal resolution is 1° × 1° for the SST and GPCC precipitation datasets and 2.5° × 2.5° for the wind and CMAP precipitation datasets. We also use the subsurface ocean temperature and ocean currents from the Global Ocean Data Assimilation System (GODAS) (Behringer and Xue 2004) at a horizontal resolution of 1° longitude × 1/3° latitude.

### b. Methods

Anomalies for all variables are computed by removing the monthly mean climatology (1971–2017). The linear trends were removed from all datasets to avoid possible influences associated with global warming. The Niño-3.4 index, the area-averaged SSTAs in the Niño-3.4 region (5°S–5°N, 120°–170°W), is used to measure ENSO intensity. El Niño events are identified according to Climate Prediction Center's definition. If the 3-month running mean of the Niño-3.4 index is larger than 0.5°C for five consecutive months, this year will be categorized as an El Niño year. With this method we identify 13 El Niño events (Table 1). We further identify EP and CP El Niño events based on the cold tongue ($N_{CT}$) and warm pool ($N_{WP}$) indices (Ren and Jin 2011), respectively (Table 1), with $N_{CT}$ and $N_{WP}$ defined as follows:

$$\begin{cases} N_{CT} = N_3 - \alpha N_4 \\ N_{WP} = N_4 - \alpha N_3 \end{cases}, \alpha = \begin{cases} 0.4, N_3 N_4 > 0 \\ 0, \text{otherwise} \end{cases}. \quad (1)$$

Here $N_3$ and $N_4$ denote Niño-3 and Niño-4 indices, which are defined as the area-averaged SSTAs in the Niño-3 (5°S–5°N, 90°–150°W) and Niño-4 (5°S–5°N, 120°–170°W) region, respectively. The El Niño events with $N_{WP}$ greater than $N_{CT}$ are defined as CP El Niño events while those with $N_{CT}$ greater than $N_{WP}$ are identified into EP El Niño events. For some events with comparable $N_{WP}$ and $N_{CT}$ (1986 and 1991), we classify them into CP events considering that the central Pacific SSTAs are much easier to excite convection here and have climate impacts over East Asia similar to the typical CP El Niño events (Zhang et al. 2013, 2014). To measure the intensity of Indian Ocean (IO) basin warming during the El Niño decaying phase, an IO index is calculated as an area average of the SSTAs in the region of 10°S–10°N and 40°–100°E (Xie et al. 2009). Based on our previous work (Zhang et al. 2015), the C-mode index is defined as the zonal surface wind difference between the southeastern equatorial Pacific (0°–10°S, 120°–170°W) and the northwestern equatorial Pacific (0°–10°N, 120°–170°E). To extract the contribution of local (non-C-mode-related) WNP SST cooling to the SPSC, we remove the temperature signal from C-mode induced air–sea interactions from the area-averaged SSTAs in the WNP (0°–15°N, 120°–160°E) via linear regression (referred to as the WNP index). To avoid the possible influence of the decadal signal of CP El Niño (e.g., Ren and Jin 2013), we also apply a 3–120-month filter to each dataset and find that our main conclusion remains almost the same. All statistical significance tests are performed using the two-tailed Student's $t$ test (Wilks 2006).

### c. Model simulations

The numerical model used here is the Geophysical Fluid Dynamics Laboratory (GFDL) Global Atmospheric Model version 2.1 (AM2.1) at a horizontal resolution of 2.5° longitude × 2° latitude. The seasonal varying climatological SSTs were used as the forcing to obtain the climatological state (CTRL). Two sensitivity experiments (EXP-WCP and EXP-DCP) were conducted with the composite SSTAs of the wet and dry CP El Niño over the tropical Pacific (20°S–20°N, 150°E–90°W) from February to April, respectively (similar results can be obtained by forcing from February to May). SSTAs outside the forcing area were set to zero and only the positive loading in the region was used. Each run was integrated for 30 years, and the output from the last 20 years of the integration was averaged to reduce the possible impact of the internal variability.

## 3. Different SPSC characteristics for different El Niño flavors

Figure 1 shows composite SPSC anomalies during the decaying spring phase [March–May (MAM)] of all El Niño, EP El Niño, and CP El Niño events. Southern China usually experiences a wetter than normal spring when El Niño occurs (Fig. 1a), consistent with previous studies (Wang et al. 2000; Feng et al. 2011). However, there are contrasting SPSC characteristics between EP and CP El Niño events. EP El Niño events are often accompanied by pronounced positive precipitation anomalies over southern China (Fig. 1b), whereas almost no statistically significant precipitation responses are detected during the decaying spring of CP El Niño events (Fig. 1c). Similar results can also be obtained

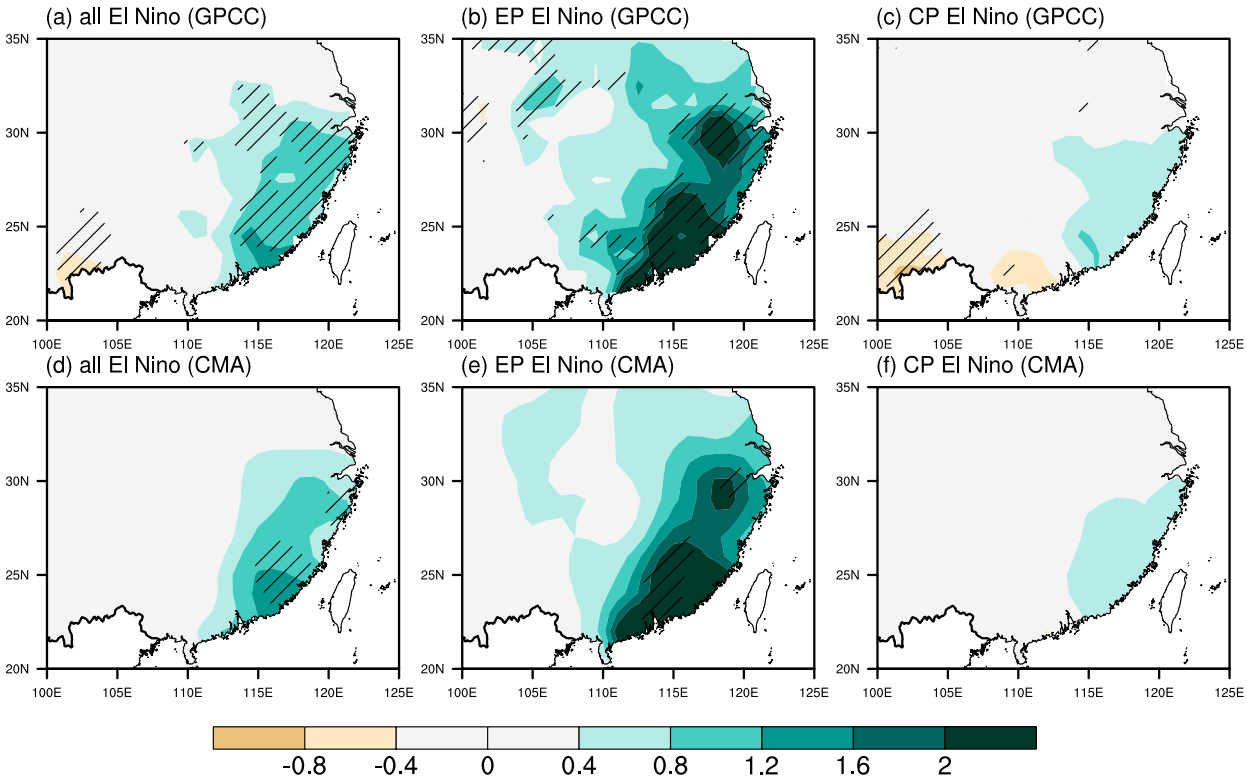


FIG. 1. Spatial distribution of the composite GPCC precipitation anomalies (mm day$^{-1}$) during the decaying spring phase of (a),(d) all El Niño, (b),(e) EP El Niño, and (c),(f) CP El Niño events by using the (top) GPCC and (bottom) CMA datasets. Hatching indicates composite values that exceed the 90% significance level.

by using the station precipitation data from CMA (Figs. 1d–f)

To further investigate the relationship between SPSC and El Niño, a SPSC index is defined as an area average of the precipitation anomalies over southern China (20°–30°N, 107.5°–120°E), where the spring precipitation accounts for around 35% of the annual total and has a large standard deviation (Wu et al. 2003; Feng et al. 2011). The qualitative conclusions remain the same for slight changes in the area (such as 105°–120°E or 110°–120°E). As shown in Fig. 2a, all the EP El Niño events are accompanied by precipitation surplus over southern China during decaying spring, suggesting a robust relationship between EP El Niño and SPSC. However, the picture is much more complicated when looking at CP El Niño events. Around half the CP events (5 of 9; i.e., 1977/78, 1979/80, 1986/87, 1991/92, 2009/10) correspond to a positive SPSC index, while the other half (4 of 9; i.e., 1994/95, 2002/03, 2004/05, 2006/07) are associated with a negative SPSC index (the EP events are also shown as reference). It seems that these CP El Niño events naturally fall into two groups, one associated with a precipitation surplus (wet CP El Niño hereafter) and the other with a precipitation deficit (dry CP El Niño hereafter) in the region. The composite SPSC responses for these CP El Niño types further highlight their distinct precipitation anomalies over southern China (Figs. 2b,c).

## 4. Different SSTA evolutions for the wet and dry CP El Niño events

It is compelling to ask whether the wet and dry CP El Niño events exhibit different SSTA structures in the tropical Pacific. To answer this scientific issue, we compare the tropical SSTA patterns associated with wet and dry CP El Niño and EP El Niño events in terms of their intensity and zonal position (Fig. 3). Compared to the EP El Niño composite with positive SSTAs centered around 120°W, the two types of CP El Niño have SSTA centers that are shifted westward to the central Pacific and weaker amplitude. For the wet CP El Niño, the positive SSTAs are located in the central-eastern Pacific during the entire period and reach their largest amplitude around December(0). The maximum SSTA center is mainly confined to the east of 160°W with no pronounced longitudinal migration during the time evolution of the event. During dry CP El Niño developing

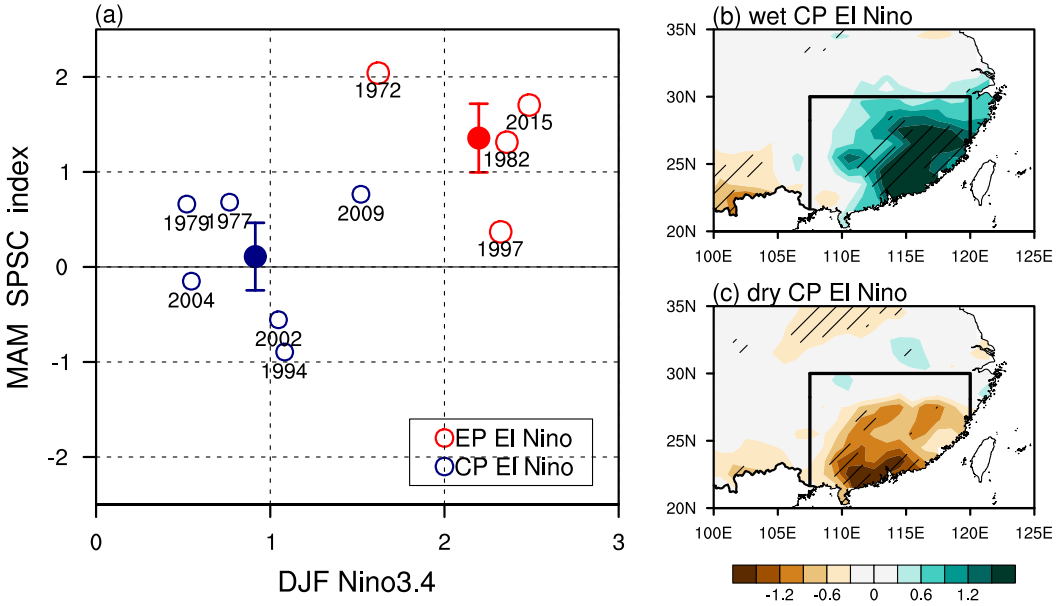


FIG. 2. (a) Scatterplot between MAM SPSC and preceding DJF Niño-3.4 (°C) indices for EP (red hollow circle) and CP El Niño (blue hollow circle) events. Solid circles denote the corresponding composite values. Red and blue error bars represent 0.5 standard deviation error estimates for EP and CP events, respectively. The spatial distribution of the composite GPCC precipitation anomalies (mm day$^{-1}$) during decaying spring of (b) wet and (c) dry CP El Niño events. Hatching indicates composite values that exceed the 90% significance level. Years in all scatterplots indicate the developing year of each El Niño event (e.g., 2002 indicates the 2002/03 El Niño event).

autumn and mature winter positive SSTAs are also present in the central-eastern Pacific, which resembles the wet CP El Niño pattern but with a westward displacement of the maximum SSTAs (Fig. 3b). However, after January(1), the maximum SSTA center of the dry CP El Niño propagates westward to the central-western Pacific, while rapidly decaying in amplitude. During decaying spring phase, the tropical Pacific shows a positive and negative SSTA dipole between the central-western and eastern Pacific, different from the wet CP El Niño pattern during this season.

To further demonstrate the SSTA differences associated with the two types of CP El Niño events, we examine the SSTA distribution along the equator for wet and dry CP El Niño, as well as for EP El Niño, from the developing autumn to decaying spring phase (Fig. 4). From the developing autumn to mature winter EP El Niño exhibit maximum SSTAs in the eastern equatorial Pacific. In contrast, the CP El Niño's SSTA center is located around 160°W. The two types of CP El Niño are similar during this phase and cannot be clearly distinguished by their equatorial SSTA pattern. However, during the decaying spring phase, wet and dry CP El Niño events are easily separated according to their different equatorial SSTA patterns. The equatorial SSTA structure of wet CP El Niño is similar to that of EP El Niño, characterized by relatively high positive SSTAs in the eastern Pacific. In contrast, the SSTA amplitude of the dry CP El Niño is reduced to be about half of the wet CP event amplitude, and the longitudinal location of its anomaly center is shifted westward by ~40° compared to the position during wet CP events. In addition, the far eastern Pacific shows negative SSTAs during this phase of dry CP events. These results show distinct SSTA patterns for wet and dry CP events during the decaying spring, especially in their amplitude and longitudinal position (Fig. 5).

To further confirm that different SSTA patterns associated with the wet and dry CP El Niño events (Figs. 6a,b) are responsible for different SPSC responses, two sensitivity experiments (EXP-WCP and EXP-DCP) are conducted (see experimental designs in section 2). Figures 6c and 6d show differences in low-level wind and precipitation in the EXP-WCP and EXP-DCP runs relative to the CTRL run. In the EXP-WCP experiment, an anomalous anticyclone is forced over the WNP, which transports more moisture to southern China and thus causes more SPSC (Fig. 6c). In contrast, the dry CP El Niño–associated SSTAs (the EXP-DCP experiment) in the tropical Pacific, can produce an anomalous cyclonic circulation over the WNP and thus the northeasterly wind anomalies prevail over south China, inhibiting moisture transported into China and leading to less SPSC. It

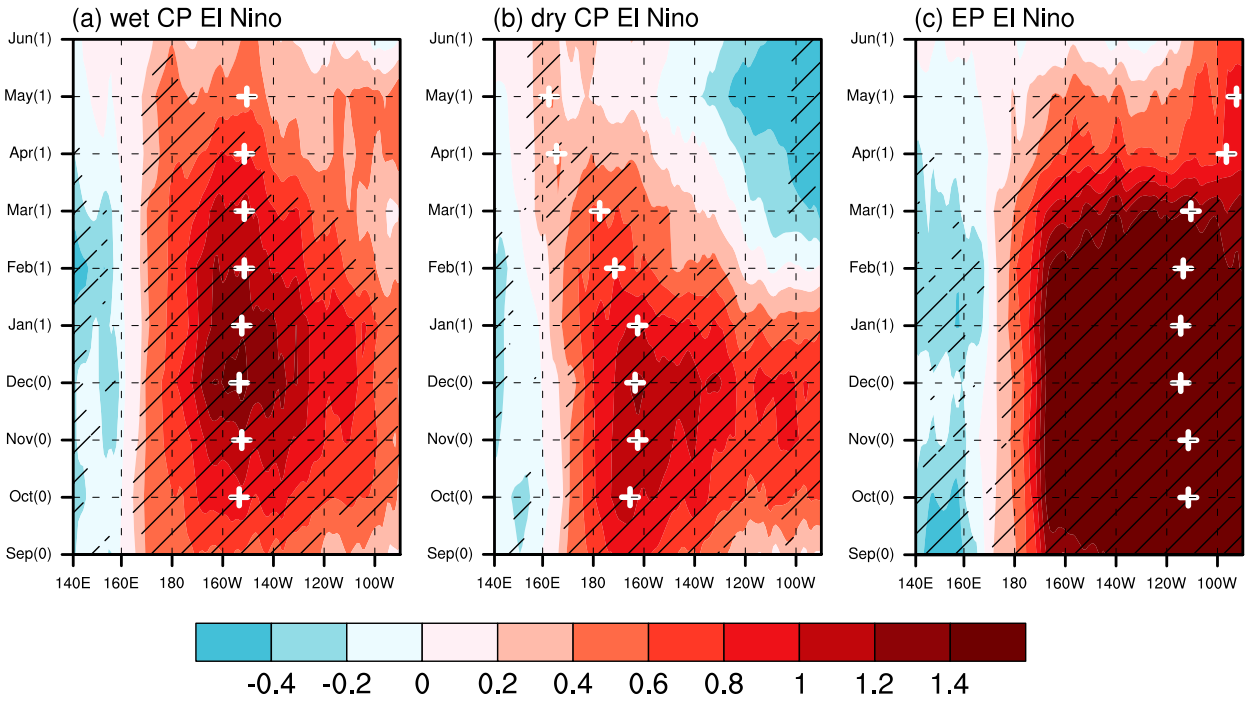


FIG. 3. Time–longitude sections of the composite equatorial (5°S–5°N) SSTAs (°C) for (a) wet CP El Niño, (b) dry CP El Niño, and (c) EP El Niño events. Numerals "0" and "1" in the ordinate denote El Niño developing and decaying years, respectively. Hatching indicates composite values that exceed the 90% significance level. White crosses mark the longitudinal positions of the maximum SSTAs.

can be seen that the tropical Pacific SST forcing can well simulate the observed responses, which further confirm that the different CP El Niño types can produce the different WNP atmospheric anomalies and thus different SPSC.

During wet CP El Niño decaying spring, corresponding to the high positive SSTAs in the central-eastern Pacific and negative SSTAs in the WNP, westerly wind anomalies are observed with a maximum south of the equator at around 5°S (Fig. 5), resembling the positive phase of the C-mode wind pattern (Stuecker et al. 2013; Stuecker et al. 2015; Zhang et al. 2015). In contrast, during the same phase of dry CP El Niño events, positive SSTAs are confined to the central equatorial Pacific around the date line, with negative SSTAs in the eastern equatorial Pacific. Meanwhile, the negative SSTAs over the WNP are much weaker compared to anomalies in this region during wet CP events. Correspondingly, no clear C-mode wind pattern is evident during this phase of dry CP events.

## 5. Possible mechanisms for the distinct precipitation responses

In the previous sections we showed that the two types of CP El Niño events show distinct tropical SSTA evolutions and associated atmospheric circulation characteristics. The next question remaining to be answered is how these two different CP El Niño types bring about different SPSC responses. According to previous studies, the C-mode is the prime driver for the development of an anomalous low-level anticyclone over the WNP region during the El Niño decaying phase (Stuecker et al. 2013, 2015), which usually transports more moisture to East Asia and thereby causes more precipitation over southern China (Zhang et al. 2015). This relationship is very robust for EP El Niño events; however, for CP El Niño, the C-mode response shows typically a more meridionally symmetric wind pattern (absence of an anticyclonic WNP circulation) (McGregor et al. 2013) and there is no clear SPSC response evident during the decaying spring phase (Zhang et al. 2016). The tropical atmospheric responses during the two types of CP El Niño decaying spring phase manifest distinct C-mode features, which may provide some clue to explain their different impacts on the SPSC (Fig. 5).

We next investigate the temporal evolution of C-mode indices (i.e., the aforementioned metric for a meridionally antisymmetric surface wind response) from September(0) to June(1) for the wet and dry CP El Niño events (Fig. 7a). For wet CP El Niño, the composite C-mode index is negative during the developing

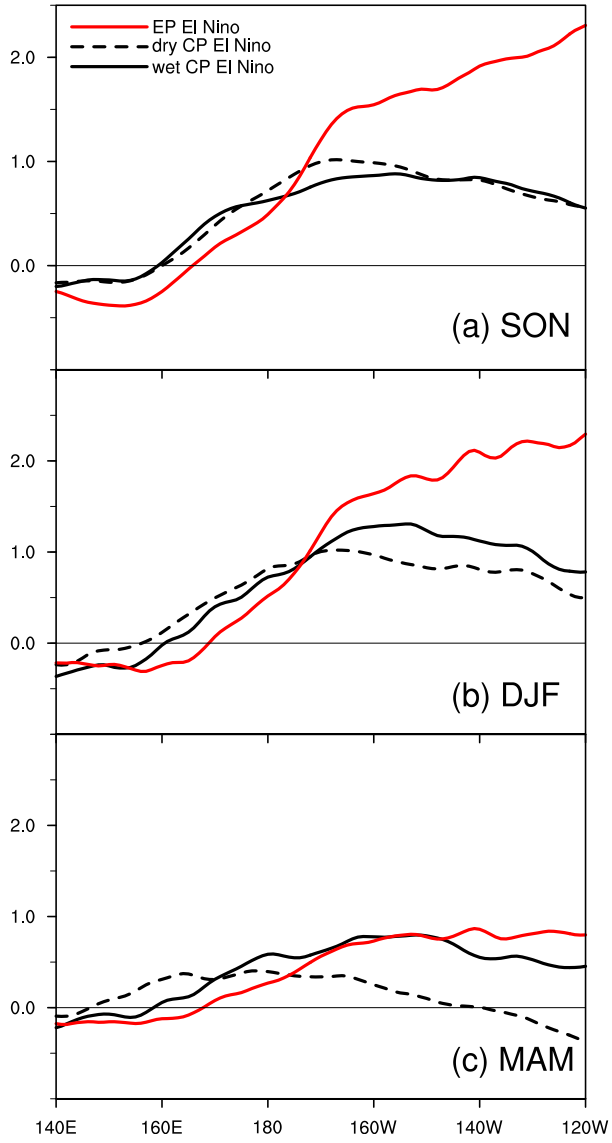


FIG. 4. Zonal distributions of SSTAs (°C) along the equator (5°S–5°N) that are smoothed zonally using a 5-point running mean of wet CP El Niño (black solid line), dry CP El Niño (black dashed line), and EP El Niño (red solid line) composites during (a) developing autumn, (b) mature winter, and (c) decaying spring.

phase and then reverses its sign to positive after November. It reaches its peak value in decaying March, indicating the location of central Pacific westerly wind anomalies to the south of the equator during this season (McGregor et al. 2012; Stuecker et al. 2013). The time evolution is similar for all the five events despite some differences in their relative amplitude. However, for the dry CP El Niño events, from the developing autumn to the decaying spring, the composited C-mode index remains at negative values. All the four dry CP El Niño events exhibit a similar time evolution of the C-mode index. The remarkable differences in C-mode responses during the decaying phase of these two types of CP El Niño can be further confirmed by a scatterplot between the C-mode and SPSC induces (Fig. 7b). Here we show the February–April (FMA) C-mode index since the C-mode pattern generally reaches its largest amplitude during the early spring (Stuecker et al. 2015; Zhang et al. 2015). These two indices exhibit a strongly linear relationship with a correlation coefficient of 0.89 (exceeding the 99% significance level). The C-mode indices are positive for all wet CP El Niño and negative for all dry CP El Niño events. These results further indicate that distinct SPSC responses to the two types of CP El Niño can be largely attributed to the C-mode; that is, the characteristic meridionally asymmetric C-mode wind pattern (and corresponding anomalous anticyclonic WNP circulation) is absent for dry CP El Niño events.

To better understand different C-mode anomalies associated with the two types of CP El Niño, we composite the monthly evolution of zonal mean (140°E–140°W) wind anomalies during the wet and dry CP El Niño events, respectively (Fig. 8), following our previous study (Zhang et al. 2015). The central Pacific (140°E–140°W) region is chosen because in this region the combination of ENSO SSTAs and high background SSTs can easily excite atmospheric convection anomalies. For wet CP El Niño events, the equatorial westerly anomalies develop rapidly during the developing autumn season, and then shift to the south of the equator in next few months. These westerly anomalies prevail at about 5°S during the decaying spring phase. This characteristic evolution of the westerly anomalies is absent for the dry CP events (Fig. 8b). Instead, even during the decaying spring, there exists a weak easterly wind south of the equator in the central Pacific. The C-mode associated southward wind shift of westerly anomalies has been suggested to be associated with anomalous convection. The enhanced precipitation south of the equator during the spring season results in pronounced atmospheric subsidence north of the equator, especially over the WNP, which contributes to the enhancement of SPSC (Stuecker et al. 2015; Zhang et al. 2015).

To further explore the different wind responses to convection anomalies for wet and dry CP El Niño, we show the composite precipitation, wind, and SSTAs over the tropical Pacific during the decaying FMA season (Fig. 9). Because of the annual cycle of solar radiation, the climatological SSTs exhibit a high meridional asymmetry with regards to the equator in the warm pool region. High climatological SSTs are mainly located south of the equator with the South Pacific convergence zone (SPCZ) extending eastward to ~130°W during the spring season. For the wet CP El Niño, the meridionally

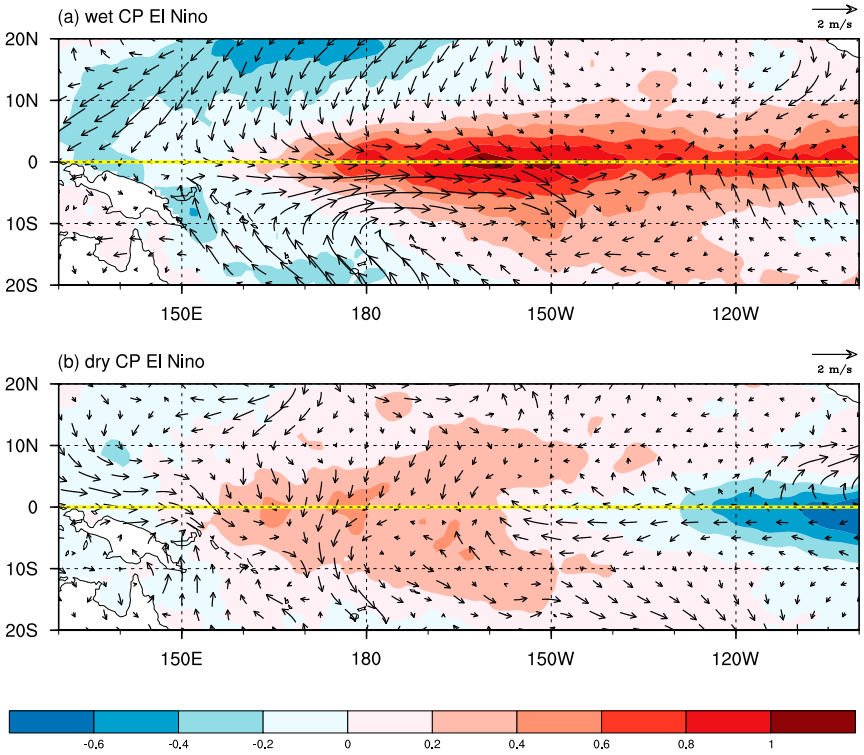


FIG. 5. Composite SST (°C) and 850-hPa wind (m $s^{-1}$) anomalies during (a) wet and (b) dry CP El Niño decaying spring.

quasi-symmetric positive ENSO SSTAs extend from the coast of South America to about 165°E during the decaying spring phase (Fig. 9a). These quasi-symmetric positive SSTAs superimposed on the meridionally antisymmetric background SSTs lead enhanced convection and precipitation in the southern part of the central Pacific and increased subsidence and decreased precipitation in the WNP. Over the WNP, negative local

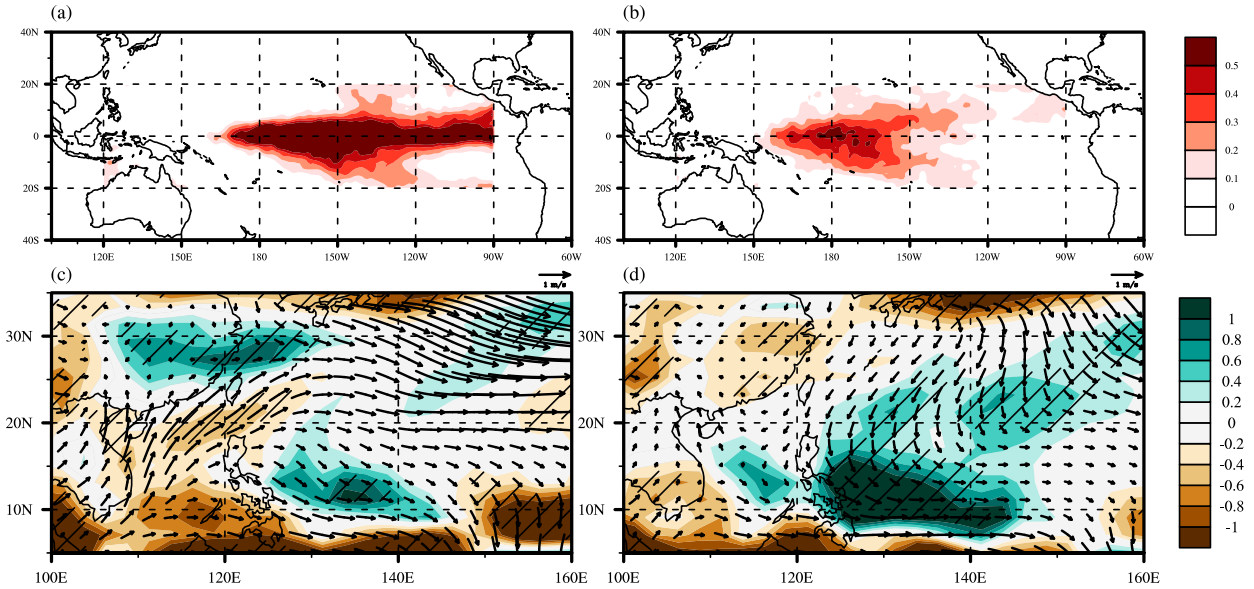


FIG. 6. (top) Averaged SST anomaly patterns specified in the (a) EX-WCP run and (b) EX-DCP run from decaying January to April. (c),(d) Ensemble-mean spring (MAM) response of 850-hPa wind (vectors; m $s^{-1}$) and precipitation (shading; mm $day^{-1}$) to the tropical Pacific SST forcings in (a) and (b), respectively. Hatching indicates composite precipitation that exceeds the 90% significance level.

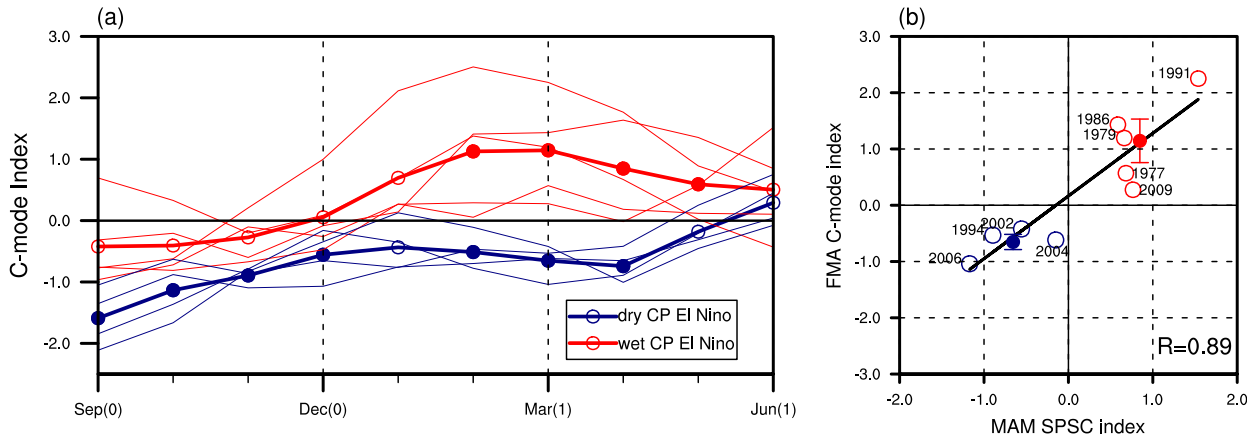


FIG. 7. (a) Monthly evolutions of the C-mode index (3-month running mean) during the wet (thin red lines) and dry (thin blue lines) CP El Niño events. Solid circles indicate the composite values (thick lines) that exceed the 90% significance level. (b) Scatterplot of the FMA C-mode index with the MAM SPSC index during the wet (red hollow circle) and dry CP El Niño (blue hollow circle) events. Solid circles denote the corresponding composite values for the wet and dry CP El Niño events, respectively. Error bars represent 0.5 standard deviation error estimates for the wet and dry CP El Niño events, respectively.

SSTAs can further reduce convection and precipitation here and reinforce the anticyclonic circulation anomalies (Wang et al. 2000).

During the dry CP El Niño decaying season, the SSTAs are highly symmetric about the equator, small in amplitude, and displaced westward compared to wet CP El Niño events (Fig. 9b). Although the background SSTs are slightly warmer south of the equator than north of the equator in the far western tropical Pacific, the climatological SSTs north of the equator are still around 28°C, exceeding the threshold for deep convection (Fig. 9b). In this case, the westward shift of warm SSTAs can easily excite strong convection anomalies both to the north and south of the equator, and the associated precipitation anomalies are highly symmetric about the equator. Consequently, no strong meridional shift of zonal wind anomalies is observed in the central Pacific. As a response to the positive convection anomalies over the western Pacific, cyclonic wind anomalies over the WNP reduce the moisture transport from the tropical oceans to southern China and result in a decrease of SPSC.

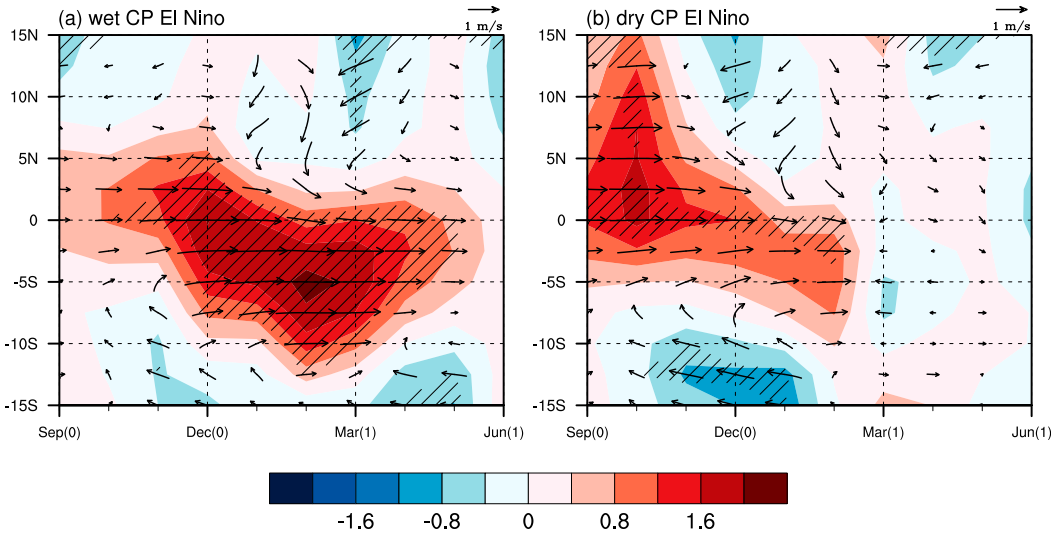


FIG. 8. Latitude–time sections of zonal mean (140°E–140°W) 10-m wind anomalies (vectors; m $s^{-1}$) for the (a) wet and (b) dry CP El Niño event composites. The shading displays the corresponding zonal 10-m wind anomalies (m $s^{-1}$). Hatching indicates composite values that exceed the 90% significance level.

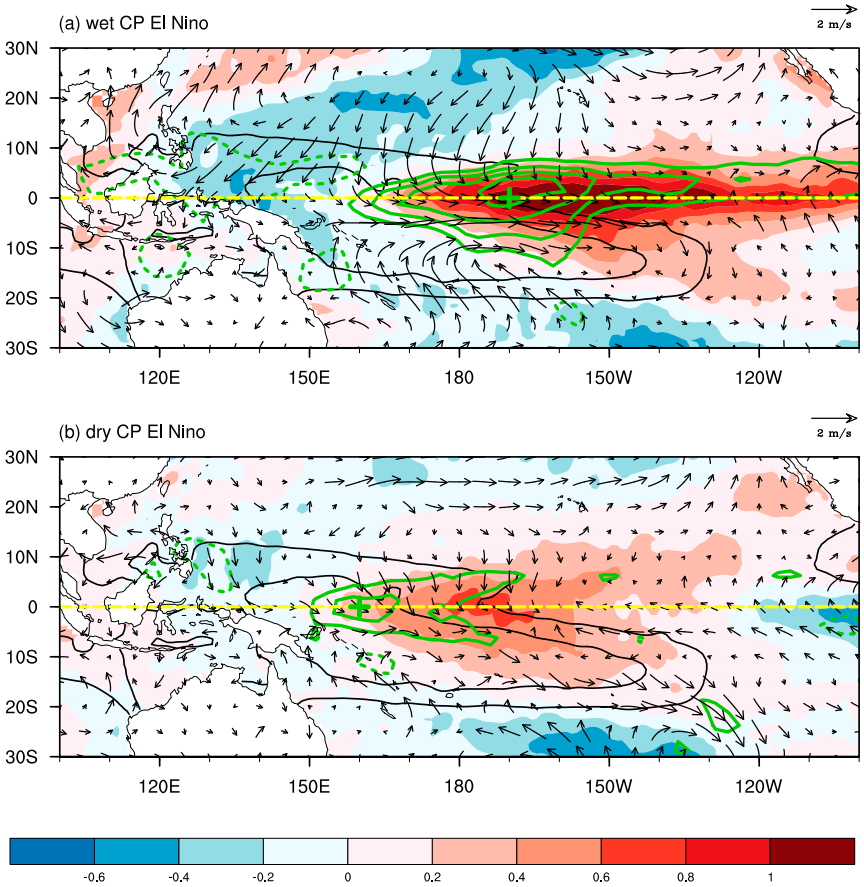


FIG. 9. Composite FMA-mean SSTAs (shadings; °C), precipitation anomalies (green contours at intervals of 1.5 mm day$^{-1}$ with zero contours omitted), and 10-m wind anomalies (vectors; m s$^{-1}$) for (a) wet and (b) dry CP El Niño event composites. Black contours display the climatological FMA-mean SST at 28° and 29°C.

To quantify the effect of the positive SSTA longitudinal position on the SPSC response, we show a scatterplot of the SPSC index with the longitudinal position of the maximum SSTAs averaged from 5°S to 5°N (between 140°E and 140°W) (Fig. 10). A statistically significant positive linear relationship can be detected ($r = 0.67$, exceeding the 95% significance level). It suggests that the MAM SPSC responses to CP El Niño events are closely related to the longitudinal position of positive equatorial SSTAs. Besides, the correlation coefficient between the FMA C-mode index and the longitudinal SSTA position is 0.63, which exceeds the 90% significance level (not shown). Therefore, the SSTA longitudinal position during different CP El Niño events largely determines the C-mode response, which in turn is responsible for the different SPSC responses.

## 6. Conclusions and discussion

Previous studies suggested that the SPSC responses to different El Niño events vary and that the El Niño type should be taken into consideration (Feng et al. 2011; Feng and Li 2011). During the EP El Niño decaying spring phase, there typically exists a prominent low-level anticyclonic atmospheric circulation in the WNP that is associated with the C-mode (Stuecker et al. 2013, 2015). This WNP anticyclone favors increased moisture transport to East Asia and thus results in enhanced precipitation over southern China (Wang et al. 2000; Feng and Li 2011). In contrast, the SPSC responses to CP El Niño are controversially debated in previous studies (Feng et al. 2011; Feng and Li 2011). Here we showed that while one type of CP event is accompanied by enhanced SPSC (wet CP El Niño), a second type is associated with reduced SPSC (dry CP El Niño). We find that distinct C-mode responses are largely responsible for different SPSC responses to the wet and dry CP El Niño events. Furthermore, the C-mode and SPSC responses are closely associated with the SSTA longitudinal position during the CP El Niño decaying spring phase. Because of the different meridional structure of

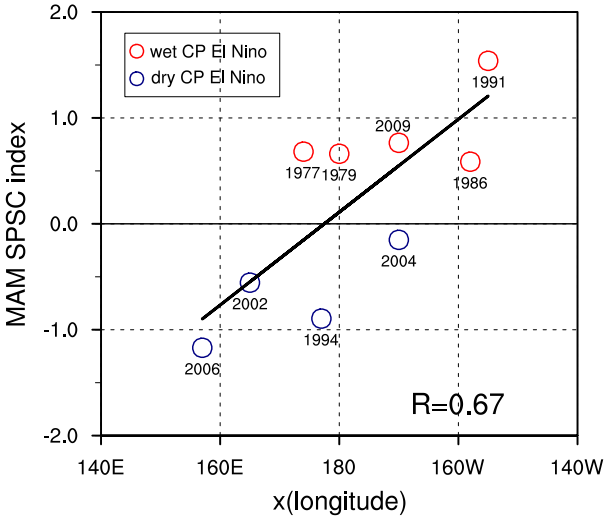


FIG. 10. Scatterplot of the MAM SPSC index with the MAM zonal location of maximum SSTAs averaged from 5°S to 5°N during the wet (red hollow circle) and dry CP El Niño (blue hollow circle) events.

climatological SSTs in the tropical far western and central Pacific, the different longitudinal position of positive SSTAs leads to different meridional structures of convective anomalies, which in turn cause distinct C-mode responses and therefore different SPSC responses.

It is emphasized in previous studies that the potential roles of local air–sea interaction in the WNP (Wang et al. 2000) and Indian Ocean delayed warming (Yang et al. 2007) for the atmospheric WNP and SPSC responses to ENSO. However, it remains unclear to what extent these two processes contribute to SPSC anomalies during the decaying phase of CP El Niño events. Here we discuss possible influences associated with the Indian Ocean (IO) and WNP indices on the SPSC during the decaying spring phase of the two types of CP El Niño events. It has been demonstrated that the C-mode atmospheric circulation pattern is mainly responsible for remote SSTA changes, specifically cooling in the WNP region (Stuecker et al. 2015; Zhang et al. 2016). Thus, we next remove the C-mode-induced signal from the WNP SSTAs using linear regression (see section 2) to examine the effect of local non-C-mode-related WNP SSTAs on the atmospheric circulation anomalies. We find no statistically significant linear relationship between the SPSC anomalies with both the IO and WNP SSTAs (Fig. 11). Different from the C-mode index, the composite values of these two indices in the wet and dry CP El Niño events are both of same sign, which fails to account for the distinct SPSC responses. It is also supported by our modeling experiments, in which we do not specify cold SSTAs in the WNP and warm SSTAs in the IO, and avoid the possible impact of cold WNP and warm IO SSTAs. The observed differences in the WNP circulation and SPSC associated with wet and dry CP El Niño can be well simulated by the modeling experiments.

In addition, it remains unclear why CP El Niño events evolve into different SSTA patterns in the decaying spring from similar previous tropical SSTA patterns. To figure out possible reasons, we conduct heat budget analyses in the eastern Pacific (5°S–5°N, 100°W–180°) for the wet and dry CP El Niño (Fig. 12) following Jin et al. (2006):

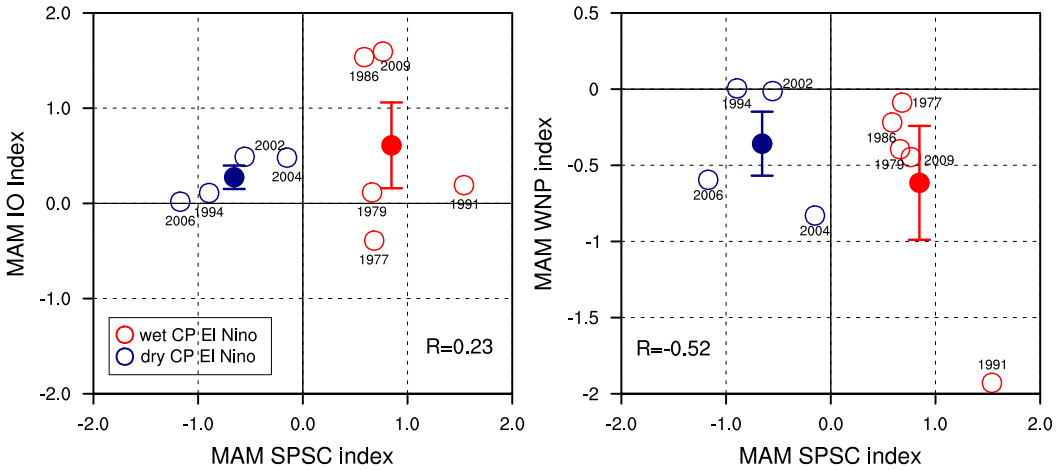


FIG. 11. Scatterplots of the MAM (a) IO and (b) WNP index with the MAM SPSC index during the wet (red hollow circle) and dry CP El Niño (blue hollow circle) events. Solid circles denote the corresponding composites for the different CP El Niño events. Error bars represent 0.5 standard deviation error estimates for the wet and dry CP El Niño events, respectively.

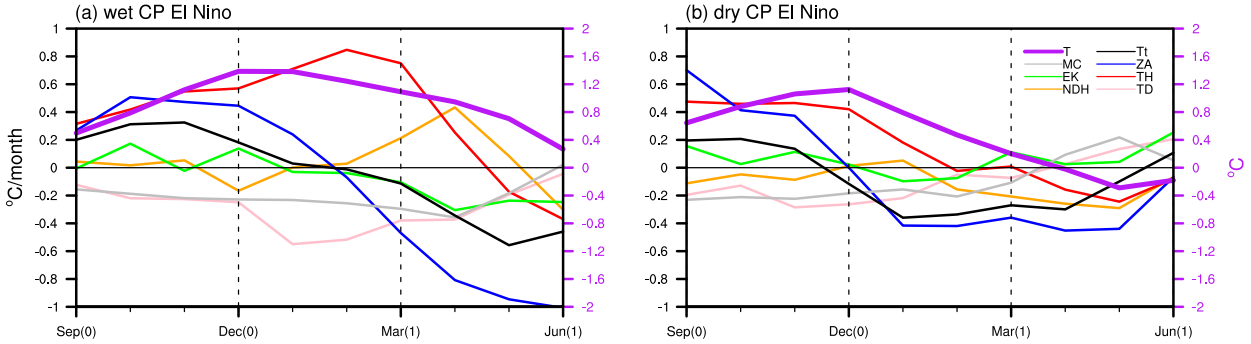


FIG. 12. Mixed layer temperature budget of (a) wet and (b) dry CP El Niño composites in the eastern Pacific (5°S–5°N, 100°W–180°). Temperature anomalies are plotted using the scale of the right axis. Purple, black, gray, blue, green, red, orange, and pink lines represent the *T*, Tt, MC, ZA, EK, TH, NDH, and TD terms, respectively.

$$\mathrm{Tt} = \mathrm{MC} + \mathrm{ZA} + \mathrm{EK} + \mathrm{TH} + \mathrm{NDH} + \mathrm{TD} + R, \quad (2)$$

where Tt denotes the mixed layer (5–45 m) averaged temperature tendency, MC the effect of mean circulation, ZA the zonal advective feedback, EK the Ekman pumping feedback, TH the thermocline feedback, NDH the nonlinear dynamical heating, TD the thermodynamical damping, and *R* the residual. Note that two CP El Niño events (1977 and 1979) are not included because GODAS data are only available since 1981. For the dry CP El Niño, the ZA term turns its phase from a positive to negative contribution around December. In contrast, the wet CP El Niño is lagged by about two months. From January to April, the ZA term for both two CP El Niño types makes a positive contribution to the decaying despite larger values for the dry than wet CP El Niño. The TH term exhibits a much bigger difference than the ZA term. In the spring, the TH term of the dry CP El Niño is reduced to near zero while the wet CP El Niño still exhibits a positive value for the TH term, which plays an important role for the slower decaying speed. It seems that the TH differences make a relatively dominant contribution to their different decaying features. This TH difference could be related to a farther westward location and weaker SSTAs for the dry than wet CP El Niño events.

In this study, we emphasize that distinct C-mode responses are largely responsible for the opposite SPSC responses to different CP El Niño flavors, which provides important information for seasonal climate predictions. However, it is undeniable that SPSC can also influenced by other factors outside the tropical Pacific (Wu and Kirtman 2007; Zheng et al. 2015; Senan et al. 2016). More research is needed to further quantify various contributions to SPSC.

*Acknowledgments.* This work was supported by the National Key Research and Development Program on Monitoring, Early Warning and Prevention of Major Natural Disaster (2018YFC1506002), the National Nature Science Foundation of China (41675073), the SOA Program on Global Change and Air–Sea interactions (GASI-IPOVAI-03), and the Institute for Basic Science (project code IBS-R028-D1).

## REFERENCES

Ashok, K., S. K. Behera, S. A. Rao, H. Weng, and T. Yamagata, 2007: El Niño Modoki and its possible teleconnection. *J. Geophys. Res. Oceans*, **112**, C11007, https://doi.org/10.1029/2006JC003798.

Becker, A., P. Finger, A. Meyer-Christoffer, B. Rudolf, K. Schamm, U. Schneider, and M. Ziese, 2013: A description of the global land-surface precipitation data products of the Global Precipitation Climatology Centre with sample applications including centennial (trend) analysis from 1901–present. *Earth Syst. Sci. Data*, **5**, 71–99, https://doi.org/10.5194/ESSD-5-71-2013.

Behringer, D. W., and Y. Xue, 2004: Evaluation of the global ocean data assimilation system at NCEP: The Pacific Ocean. *Proc. Eighth Symp. on Integrated Observing and Assimilation Systems for Atmosphere, Oceans, and Land Surface*, Seattle, WA, Amer Meteor. Soc., 11–15.

Cane, M. A., and S. E. Zebiak, 1985: A theory for El Niño and the Southern Oscillation. *Science*, **228**, 1085–1087, https://doi.org/10.1126/science.228.4703.1085.

Chang, C. P., Y. Zhang, and T. Li, 2000a: Interannual and Interdecadal variations of the East Asian summer monsoon and tropical Pacific SSTs. Part I: Roles of the subtropical ridge. *J. Climate*, **13**, 4310–4325, https://doi.org/10.1175/1520-0442(2000)013<4310:IAIVOT>2.0.CO;2.

——, ——, and ——, 2000b: Interannual and interdecadal variations of the East Asian summer monsoon and tropical Pacific SSTs. Part II: Meridional structure of the monsoon. *J. Climate*, **13**, 4326–4340, https://doi.org/10.1175/1520-0442(2000)013<4326:IAIVOT>2.0.CO;2.

Ding, Y., and J. C. L. Chan, 2005: The East Asian summer monsoon: An overview. *Meteor. Atmos. Phys.*, **89**, 117–142, https://doi.org/10.1007/s00703-005-0125-z.

Fasullo, J., 2004: A stratified diagnosis of the Indian monsoon–Eurasian snow cover relationship. *J. Climate*, **17**, 1110–1122, https://doi.org/10.1175/1520-0442(2004)017<1110:ASDOTI>2.0.CO;2.

Feng, J., and J. Li, 2011: Influence of El Niño Modoki on spring rainfall over south China. *J. Geophys. Res.*, **116**, D13102, https://doi.org/10.1029/2010JD015160.

——, W. Chen, C. Y. Tam, and W. Zhou, 2011: Different impacts of El Niño and El Niño Modoki on China rainfall in the decaying phases. *Int. J. Climatol.*, **31**, 2091–2101, https://doi.org/10.1002/joc.2217.

——, L. Yu, and D. Hu, 2014: Influence of Indian Ocean subtropical dipole on spring rainfall over China. *Int. J. Climatol.*, **34**, 954–963, https://doi.org/10.1002/joc.3732.

Fu, C. B., and X. L. Teng, 1988: Relationship between summer climate in China and El Niño/Southern Oscillation phenomenon (in Chinese). *Chin. J. Atmos. Sci.*, **12**, 133–141.

Huang, R., and Y. Wu, 1989: The influence of ENSO on the summer climate change in China and its mechanism. *Adv. Atmos. Sci.*, **6**, 21–32, https://doi.org/10.1007/BF02656915.

Jin, F.-F., 1997: An equatorial ocean recharge paradigm for ENSO. Part I: Conceptual model. *J. Atmos. Sci.*, **54**, 811–829, https://doi.org/10.1175/1520-0469(1997)054<0811:AEORPF>2.0.CO;2.

——, S. T. Kim, and L. Bejarano, 2006: A coupled-stability index for ENSO. *Geophys. Res. Lett.*, **33**, L23708, https://doi.org/10.1029/2006GL027221.

Kalnay, E., and Coauthors, 1996: The NCEP/NCAR 40-Year Reanalysis Project. *Bull. Amer. Meteor. Soc.*, **77**, 437–472, https://doi.org/10.1175/1520-0477(1996)077<0437:TNYRP>2.0.CO;2.

Kao, H.-Y., and J.-Y. Yu, 2009: Contrasting eastern-Pacific and central-Pacific types of ENSO. *J. Climate*, **22**, 615–632, https://doi.org/10.1175/2008JCLI2309.1.

Larkin, N. K., and D. E. Harrison, 2005: Global seasonal temperature and precipitation anomalies during El Niño autumn and winter. *Geophys. Res. Lett.*, **32**, L16705, https://doi.org/10.1029/2005GL022860.

Lau, K.-M., and M.-T. Li, 1984: The monsoon of East Asia and its global associations—A survey. *Bull. Amer. Meteor. Soc.*, **65**, 114–125, https://doi.org/10.1175/1520-0477(1984)065<0114:TMOEAA>2.0.CO;2.

LinHo, L. H., X. Huang, and N. C. Lau, 2008: Winter-to-spring transition in East Asia: A planetary-scale perspective of the south China spring rain onset. *J. Climate*, **21**, 3081–3096, https://doi.org/10.1175/2007JCLI1611.1.

McGregor, S., A. Timmermann, N. Schneider, M. F. Stuecker, and M. H. England, 2012: The effect of the South Pacific convergence zone on the termination of El Niño events and the meridional asymmetry of ENSO. *J. Climate*, **25**, 5566–5586, https://doi.org/10.1175/JCLI-D-11-00332.1.

——, N. Ramesh, P. Spence, M. H. England, M. J. McPhaden, and A. Santoso, 2013: Meridional movement of wind anomalies during ENSO events and their role in event termination. *Geophys. Res. Lett.*, **40**, 749–754, https://doi.org/10.1002/grl.50136.

McPhaden, M. J., S. E. Zebiak, and M. H. Glantz, 2006: ENSO as an integrating concept in Earth science. *Science*, **314**, 1740–1745, https://doi.org/10.1126/science.1132588.

Murakami, T., 1951: On the study of the change of the upper westerlies in the last stage of baiu season (rainy season in Japan). *J. Meteor. Soc. Japan*, **29**, 162–175, https://doi.org/10.2151/jmsj1923.29.5_162.

Neelin, J. D., D. S. Battisti, A. C. Hirst, F.-F. Jin, Y. Wakata, T. Yamagata, and S. E. Zebiak, 1998: ENSO theory. *J. Geophys. Res.*, **103**, 14 2261–14 2290, https://doi.org/10.1029/97JC03424.

Ng, C. H. J., G. A. Vecchi, A. G. Muñoz, and H. Murakami, 2019: An asymmetric rainfall response to ENSO in East Asia. *Climate Dyn.*, **52**, 2303–2318, https://doi.org/10.1007/S00382-018-4253-9.

Rayner, N. A., D. E. Parker, E. B. Horton, C. K. Folland, L. V. Alexander, D. P. Rowell, E. C. Kent, and A. Kaplan, 2003: Global analyses of sea surface temperature, sea ice, and night marine air temperature since the late nineteenth century. *J. Geophys. Res.*, **108**, 4407, https://doi.org/10.1029/2002JD002670.

Ren, H.-L., and F.-F. Jin, 2011: Niño indices for two types of ENSO. *Geophys. Res. Lett.*, **38**, L04704, https://doi.org/10.1029/2010GL046031.

——, and ——, 2013: Recharge oscillator mechanisms in two types of ENSO. *J. Climate*, **26**, 6506–6523, https://doi.org/10.1175/JCLI-D-12-00601.1.

Ropelewski, C. F., and M. S. Halpert, 1987: Global and regional scale precipitation patterns associated with the El Niño/Southern Oscillation. *Mon. Wea. Rev.*, **115**, 1606–1626, https://doi.org/10.1175/1520-0493(1987)115<1606:GARSPP>2.0.CO;2.

Rudolf, B., H. Hauschild, W. Rueth, and U. Schneider, 1994: Terrestrial precipitation analysis: Operational method and required density of point measurements. *Global Precipitations and Climate Change*, M. Desbois and F. Désalmand, Eds., Springer, 173–186.

Senan, R., and Coauthors, 2016: Impact of springtime Himalayan–Tibetan Plateau snowpack on the onset of the Indian summer monsoon in coupled seasonal forecasts. *Climate Dyn.*, **47**, 2709–2725, https://doi.org/10.1007/s00382-016-2993-y.

Stuecker, M. F., A. Timmermann, F.-F. Jin, S. McGregor, and H.-L. Ren, 2013: A combination mode of the annual cycle and the El Niño/Southern Oscillation. *Nat. Geosci.*, **6**, 540–544, https://doi.org/10.1038/ngeo1826.

——, F.-F. Jin, A. Timmermann, and S. McGregor, 2015: Combination mode dynamics of the anomalous northwest Pacific anticyclone. *J. Climate*, **28**, 1093–1111, https://doi.org/10.1175/JCLI-D-14-00225.1.

Tao, S., and Q. Zhang, 1998: Response of the Asian winter and summer monsoon to ENSO events. *Sci. Atmos. Sin.*, **22**, 399–407.

Terray, P., F. Chauvin, and H. Douville, 2007: Impact of southeast Indian Ocean sea surface temperature anomalies on monsoon–ENSO–dipole variability in a coupled ocean–atmosphere model. *Climate Dyn.*, **28**, 553–580, https://doi.org/10.1007/s00382-006-0192-y.

Tian, S. F., and T. Yasunari, 1998: Climatological aspects and mechanism of spring persistent rains over central China. *J. Meteor. Soc. Japan*, **76**, 57–71, https://doi.org/10.2151/jmsj1965.76.1_57.

Timmermann, A., and Coauthors, 2018: El Niño–Southern Oscillation complexity. *Nature*, **559**, 535–545, https://doi.org/10.1038/s41586-018-0252-6.

Wallace, J. M., E. M. Rasmusson, T. P. Mitchell, V. E. Kousky, E. S. Sarachik, and H. von Storch, 1998: On the structure and evolution of ENSO-related climate variability in the tropical Pacific: Lessons from TOGA. *J. Geophys. Res. Oceans*, **103**, 14 2241–14 2259, https://doi.org/10.1029/97JC02905.

Wang, B., and Q. Zhang, 2002: Pacific–East Asian teleconnection. Part II: How the Philippine Sea anomalous anticyclone is established during El Niño development. *J. Climate*, **15**, 3252–3265, https://doi.org/10.1175/1520-0442(2002)015<3252:PEATPI>2.0.CO;2.

——, R. Wu, and X. Fu, 2000: Pacific–East Asian teleconnection: How does ENSO affect East Asian climate? *J. Climate*, **13**,

1517–1536, https://doi.org/10.1175/1520-0442(2000)013<1517:PEATHD>2.0.CO;2.

——, B. Xiang, and J.-Y. Lee, 2013: Subtropical high predictability establishes a promising way for monsoon and tropical storm predictions. *Proc. Natl. Acad. Sci. USA*, **110**, 2718–2722, https://doi.org/10.1073/pnas.1214626110.

Wang, C., and X. Wang, 2013: Classifying El Niño Modoki I and II by different impacts on rainfall in southern China and typhoon tracks. *J. Climate*, **26**, 1322–1338, https://doi.org/10.1175/JCLI-D-12-00107.1.

Watanabe, M., and F. F. Jin, 2002: Role of Indian Ocean warming in the development of Philippine Sea anticyclone during ENSO. *Geophys. Res. Lett.*, **29**, 1478, https://doi.org/10.1029/2001GL014318.

Weng, H., S. K. Behera, and T. Yamagata, 2009: Anomalous winter climate conditions in the Pacific rim during recent El Niño Modoki and El Niño events. *Climate Dyn.*, **32**, 663–674, https://doi.org/10.1007/s00382-008-0394-6.

Wilks, D. S., 2006: Statistical methods in the atmospheric sciences. *Technometrics*, **38**, 402–402.

Wilson, B., 2009: An empirical seasonal prediction model of the East Asian summer monsoon using ENSO and NAO. *J. Geophys. Res.*, **114**, D18120, https://doi.org/10.1029/2009JD011733.

Wu, G., B. Zhu, and D. Gao, 1996: The impact of Tibetan Plateau on local and regional climate. *Atmospheric Circulation to Global Change*, China Meteorological Press, 425–440.

Wu, R., and B. P. Kirtman, 2007: Observed relationship of spring and summer East Asian rainfall with winter and spring Eurasian snow. *J. Climate*, **20**, 1285–1304, https://doi.org/10.1175/JCLI4068.1.

——, Z. Z. Hu, and B. P. Kirtman, 2003: Evolution of ENSO-related rainfall anomalies in East Asia. *J. Climate*, **16**, 3742–3758, https://doi.org/10.1175/1520-0442(2003)016<3742:EOERAI>2.0.CO;2.

Wu, X., and J. Mao, 2016: Interdecadal modulation of ENSO-related spring rainfall over south China by the Pacific decadal oscillation. *Climate Dyn.*, **47**, 3203–3220, https://doi.org/10.1007/S00382-016-3021-Y.

Xie, P., and P. Arkin, 1996: Analyses of global monthly precipitation using gauge observations, satellite estimates, and numerical model predictions. *J. Climate*, **9**, 840–858, https://doi.org/10.1175/1520-0442(1996)009<0840:AOGMPU>2.0.CO;2.

Xie, S.-P., K. Hu, J. Hafner, H. Tokinaga, Y. Du, G. Huang, and T. Sampe, 2009: Indian Ocean capacitor effect on Indo–western Pacific climate during the summer following El Niño. *J. Climate*, **22**, 730–747, https://doi.org/10.1175/2008JCLI2544.1.

Xin, X., T. Zhou, and R. Yu, 2010: Increased Tibetan Plateau snow depth: An indicator of the connection between enhanced winter NAO and late-spring tropospheric cooling over East Asia. *Adv. Atmos. Sci.*, **27**, 788–794, https://doi.org/10.1007/s00376-009-9071-x.

Xu, K., C. Zhu, and J. He, 2013: Two types of El Niño–related Southern Oscillation and their different impacts on global land precipitation. *Adv. Atmos. Sci.*, **30**, 1743–1757, https://doi.org/10.1007/s00376-013-2272-3.

——, Q.-L. Huang, C.-Y. Tam, W. Wang, S. Chen, and C. Zhu, 2019: Roles of tropical SST patterns during two types of ENSO in modulating wintertime rainfall over southern China. *Climate Dyn.*, **52**, 523–538, https://doi.org/10.1007/s00382-018-4170-y.

Yang, J., Q. Liu, S.-P. Xie, Z. Liu, and L. Wu, 2007: Impact of the Indian Ocean SST basin mode on the Asian summer monsoon. *Geophys. Res. Lett.*, **34**, L02708, https://doi.org/10.1029/2006GL028571.

Yu, J. Y., and S. T. Kim, 2010: Identification of central-Pacific and eastern-Pacific types of ENSO in CMIP3 models. *Geophys. Res. Lett.*, **37**, L15705, https://doi.org/10.1029/2010GL044082.

Zhang, R., A. Sumi, and M. Kimoto, 1996: Impact of El Niño on the East Asian monsoon: A diagnostic study of the '86/87 and '91/92 events. *J. Meteor. Soc. Japan*, **74**, 49–62, https://doi.org/10.2151/jmsj1965.74.1_49.

Zhang, W., F.-F. Jin, J. Li, and H.-L. Ren, 2011: Contrasting impacts of two-type El Niño over the western North Pacific during boreal autumn. *J. Meteor. Soc. Japan*, **89**, 563–569, https://doi.org/10.2151/jmsj.2011-510.

——, ——, J. X. Zhao, L. Qi, and H. L. Ren, 2013: The possible influence of a nonconventional El Niño on the severe autumn drought of 2009 in southwest China. *J. Climate*, **26**, 8392–8405, https://doi.org/10.1175/JCLI-D-12-00851.1.

——, ——, and A. Turner, 2014: Increasing autumn drought over southern China associated with ENSO regime shift. *Geophys. Res. Lett.*, **41**, 4020–4026, https://doi.org/10.1002/2014GL060130.

——, H. Li, F.-F. Jin, M. F. Stuecker, A. G. Turner, and N. P. Klingaman, 2015: The annual-cycle modulation of meridional asymmetry in ENSO's atmospheric response and its dependence on ENSO zonal structure. *J. Climate*, **28**, 5795–5812, https://doi.org/10.1175/JCLI-D-14-00724.1.

——, ——, M. F. Stuecker, F.-F. Jin, and A. G. Turner, 2016: A new understanding of El Niño's impact over East Asia: Dominance of the ENSO combination mode. *J. Climate*, **29**, 4347–4359, https://doi.org/10.1175/JCLI-D-15-0104.1.

Zheng, F., J. Li, L. Wang, F. Xie, and X.-F. Li, 2015: Cross-seasonal influence of the December–February Southern Hemisphere annular mode on March–May meridional circulation and precipitation. *J. Climate*, **28**, 6859–6881, https://doi.org/10.1175/JCLI-D-14-00515.1.

Zhou, L. T., and R. Wu, 2010: Respective impacts of the East Asian winter monsoon and ENSO on winter rainfall in China. *J. Geophys. Res.*, **115**, D02107, https://doi.org/10.1029/2009JD012502.